Frequency-dependent stiffening of semiflexible networks: A dynamical nonaffine to affine transition

E. M. Huisman,[1] C. Storm,[2] and G. T. Barkema[1,3]
[1]*Instituut-Lorentz, Universiteit Leiden, Postbus 9506, NL-2300 RA Leiden, The Netherlands*
[2]*Department of Applied Physics and Institute for Complex Molecular Systems, Eindhoven University of Technology, P.O. Box 513, NL-5600 MB Eindhoven, The Netherlands*
[3]*Institute for Theoretical Physics, Universiteit Utrecht, NL-3584 CE Utrecht, The Netherlands*
(Received 1 July 2010; revised manuscript received 10 August 2010; published 6 December 2010)

By combining the force-extension relation of single semiflexible polymers with a Langevin equation to capture the dissipative dynamics of chains moving through a viscous medium we study the dynamical response of cross-linked biopolymer materials. We find that at low frequencies the network deformations are highly nonaffine, and show a low plateau in the modulus. At higher frequencies, this nonaffinity decreases while the elastic modulus increases. With increasing frequency, more and more nonaffine network relaxation modes are suppressed, resulting in a stiffening. This effect is fundamentally different from the high-frequency stiffening due to the single-filament relaxation modes [F. Gittes and F. C. MacKintosh, Phys. Rev. E **58**, R1241 (1998)], not only in terms of its mechanism but also in its resultant scaling: $G'(\omega) \sim \omega^{\alpha}$ with $\alpha > 3/4$. This may determine nonlinear material properties at low, physiologically relevant frequencies.

DOI: 10.1103/PhysRevE.82.061902 PACS number(s): 87.16.Ka, 81.05.Lg, 87.16.dj

I. INTRODUCTION

Tissues and cells alike owe many of their key mechanical properties to cross-linked architectures of supramolecular protein polymers [1,2]. These biomaterials display remarkably rich viscoelastic characteristics, and moreover physiological stresses, strains and strain rates are such that they readily enter nonlinear regimes [3–6,8]. Indeed, many of these nonlinear properties are presumably employed to enhance and optimize tissue functionality. In the frequency domain, previous work has established the existence of various regimes: at the lowest frequencies, cross-linking proteins reversibly bind and unbind, leading to viscous behavior [8]. At very high frequencies, on the other hand, the single-filament relaxation dynamics become dominant and lead to a characteristic $\omega^{3/4}$ scaling of the stiffness with frequency [7,9], similar to the high-frequency behavior found in entangled networks [5,10,11,21]. In this paper, we explore the behavior of rigidly cross-linked networks at intermediate time scales—those on which the cross-linking proteins may be assumed to be fixed, but the frequencies are still in the regime where all single-filament modes can relax completely. In this regime, a third, fundamentally different spectrum of relaxation modes dominates: those collective modes that effect nonaffine deformations to globally minimize the elastic energy. Prior work has established that in the low-frequency limit, networks with fixed cross-links deform in a manner that suppresses single-filament stretching by such nonaffine reorientations [12–14]. These modes, however, require that polymers move relative to the embedding medium, and while they may help minimize the elastic energy they are simultaneously *dynamically* impeded by hydrodynamic friction. At relatively high frequencies, therefore, we expect these nonaffine modes to be dynamically suppressed. In this paper we focus on the transition regime—the regime where the network crosses over from nonaffine to affine. Our results for $G'(\omega)$ agree qualitatively with those reported in very recent numerical investigations [15], but expand on these in two ways: we report the first results on the *nonlinear* elastic properties and we correlate the mechanical behavior in this regime to the extent of the nonaffinity. This nonaffinity is, for the first time, studied as a function of applied external frequency and shows a convincing downward trend with increasing frequency that confirms our interpretation.

This paper is organized as follows: we begin by explaining the generation of three-dimensional (3D) semiflexible meshworks, as well as the Langevin method for implementing the relevant dynamical effects. We measure dynamical moduli for typical parameter values, and then relate it to the dynamical nonaffinity. We identify different mechanical/dynamical regimes and probe the nonlinear response at large amplitude oscillatory shear.

II. NETWORK GENERATION

Our networks consist of long filaments that are cross-linked into a network. The cross-links act as binary bonds that connect two filaments, but allow for free rotation of these filaments with respect to each other. We do not represent all monomers explicitly but integrate out all conformational degrees of freedom of the polymers in between cross-links. This yields a Hamiltonian that sums all intersegment free energies. Additionally, consecutive segments on the same filament have a strong preference for running parallelly; the Hamiltonian therefore also assigns an energetic penalty to the bending of such adjacent segments. Both of these energy contributions are derived from the semiflexible wormlike chain model, a widely used model to describe biopolymers [16,17]. The sole degrees of freedom in our system are the curvilinear length for each segment of polymer, the locations of all cross-links and the topology of the network. Starting with a random, isotropic network, we apply a large number of Monte Carlo moves that alter the network topology such that filaments with a persistent direction-

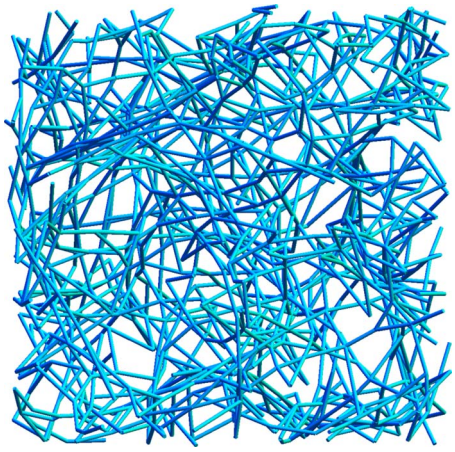

FIG. 1. (Color online) A graphical representation of one of the networks used in this study. This network consists of 333 filaments, each of which is cross-linked six times on average. The network has periodic boundary conditions in all three directions. Loose ends of the filaments are removed.

ality along segments are formed. The total generation process of each network, containing 1000 cross-links, takes up to one week of cluster computer time. We employ periodic boundary conditions. A detailed description of our simulation approach is presented in [18], together with an analysis of the network response under static shear. The primary biomaterial of our interest is cross-linked actin. Due to the time consuming method used to model the network response we restrict ourselves to averages over four individual and distinct networks with a representative set of parameters that are chosen to reflect typical networks in experiments and cells. Our networks have a protein density of 0.65 mg/ml, a persistence length ℓ_p of 16 μm and an average contour length $\langle \ell_c \rangle = 1.0$ μm between cross-links. The average length of filaments is $\langle L \rangle = 6.0$ μm and the diameter of the filaments is $b = 7$ nm. Figure 1 gives an impression of our system. Although the parameters in our simulation are chosen to reflect actin, the nonaffine-to-affine transition we identify is completely generic and qualitatively independent of parameter choices. We therefore believe our results to carry over to a wider range of biopolymer networks.

III. NETWORK DYNAMICS

We model the dynamics of these networks by connected segments that are dragged through a viscous medium and experience random thermal forces due to collisions with solvent molecules. We neglect the spatial and temporal correlations of these collisions, and effectively impose Rouse dynamics. At the intermediate time scales that we are interested in, the cross-linkers do not move along the filaments and we do not take into account the binding and unbinding of linker proteins. The elasticity of individual segments is taken to obey the semiflexible wormlike chain (WLC) model, which takes into account the thermal fluctuations of the internal degrees of freedom of the individual segments. Note that we do not keep track of these internal degrees of freedom, but replace the actual thermal semiflexible WLC by a nonlinear spring with an identical force-extension relation. Again, we are allowed to do so because of the intermediate frequency regime we explore: we make sure that frequencies do not significantly exceed the slowest single-filament mode. The dynamics of a segment in a viscous medium at finite temperature may be described by the Langevin equation,

$$\zeta \cdot \vec{v} = \vec{F} + \vec{f}_{\text{th}}, \tag{1}$$

where ζ is the drag tensor of the segment and $\vec{v}$, $\vec{F}$, and $\vec{f}_{\text{th}}$ are three-dimensional vectors representing, respectively, the velocity of the segment, the elastic force on the segment and the random thermal force on the segment. To calculate the drag on the segments, we assume the segments to be slender rods with diameter b. The drag tensor encodes the dependence of the drag coefficient on the orientation of a rod and, in addition, depends on the length ℓ_c of the rod and the viscosity of the medium, which we take to be water with $\eta = 10^{-3}$ Pa s. The axial drag coefficient $\zeta_\parallel$, the perpendicular drag coefficient $\zeta_\perp$ and the rotational drag coefficient $\zeta_\top$ are then respectively given by [19]

$$\zeta_\parallel = \frac{2\pi\eta\ell_c}{\ln(\ell_c/b)}, \quad \zeta_\perp = \frac{4\pi\eta\ell_c}{\ln(\ell_c/b)}, \quad \zeta_\top = \frac{\pi\eta\ell_c^3}{3\ln(\ell_c/b)}. \tag{2}$$

In our simulations, we discretize Eq. (1) for small steps Δt as

$$\vec{x}_i(t+\Delta t) = \left\langle \frac{F_\parallel}{\zeta_\parallel} + \frac{F_\perp}{\zeta_\perp} + \frac{(\vec{r}_i \times F_\top) \times \vec{r}_i}{\zeta_\top} + \frac{2F_s}{\zeta_\parallel} \right\rangle \Delta t + g_\parallel + g_\perp + g_\top + g_s + \vec{x}_i(t), \tag{3}$$

where $\vec{x}_i(t)$ is a three-dimensional vector representing the coordinates of the center of mass of the segment in the network at time t. The computer program keeps track of the cross-linker positions; the position x_i of segment i is simply the average of the positions of the two cross-linkers at the ends of this segment, and the end-to-end vector $\vec{r}_i$ of segment i is the difference in these cross-linker positions. $F_\parallel$ is the force along the filament, $F_\perp$ the force perpendicular to the segment, $F_\top$ the force that rotates the filament and F_s the force that stretches/compresses the filament. Note that the drag coefficient of this compressional force is half of the axial drag coefficient. The thermal random force f_{th} is represented by $\vec{g}$, a Gaussian fluctuation with standard deviation s. To ensure proper statistical sampling, we choose $s_i = \sqrt{\frac{2k_B T \Delta t}{\zeta_i}}$ which ensures that detailed balance is obeyed in the limit of small time steps.

The size of the time step Δt is determined by the stiffest mode and depends on the length of the segments. In our networks we typically take $\Delta t = 0.1$ ns. After generation we thermalize our networks during 0.1 s—we assume that all relevant length scales are relaxed in that time.

Inherent to this simulation approach is the assumption that the internal degrees of freedom of individual segments are equilibrated at all times. Based upon the behavior of a single WLC, the dispersion relation may be computed to be [7]

$$\omega(q_n) = \frac{\kappa}{\zeta} q_n^4 = \frac{\kappa}{\zeta}\left(\frac{n\pi}{\ell_c}\right)^4. \tag{4}$$

Here, κ is the bending stiffness, from which the persistence length may be extracted as $\ell_p = \kappa/(k_B T)$, and ℓ_c is the segment length. At frequencies $\omega \gg \omega(q_1)$, clearly, the assumption of fully relaxed internal degrees of freedom would break down. In this regime the viscous modulus is expected to scale as $G' \sim \omega^{3/4}$ [7]. We avoid the regime where $\omega \gg \omega(q_1)$, by subdividing the segments in our networks into a finer mesh at high frequencies. Effectively, this brings the slowest internal segment modes into play—these are now explicitly tracked in our simulations. In this manner, we continue to add interpolating nodes until the relaxation times of all segments do not exceed the deformation times of the networks significantly. Typically, the number of added nodes is 5 % of the total number of nodes for $f = \omega/2\pi = 400$ Hz and 80% of the total number of nodes for $f = 40$ kHz. As a result of the added nodes, the simulation time step must be reduced while at the same time, the number of degrees of freedom increases. This renders the simulations computationally considerably more demanding, even though obviously the time per oscillation decreases linearly with frequency.

The end result is a computational model in which the single segments are purely elastic, and the network as a whole is a viscoelastic solid. In the following we analyze the dynamic viscoelastic response of these networks. We do this in a regime that precedes, but must connect up to the frequency range over which the effects of single-filament dynamics were studied in prior work [7,9].

IV. DYNAMIC MODULI IN SHEAR

In linear viscoelastic response, materials are characterized—among other equivalent representations—in terms of their dynamic moduli, the elastic modulus $G'(\omega)$ and the viscous modulus $G''(\omega)$. To measure these quantities in our simulations we apply an oscillatory shear deformation $\gamma = \gamma_0 \sin(\omega t)$ with shear amplitude γ_0, during which we monitor the motion of the segments. We also measure the shear stress in the network, defined as

$$\sigma_{xy} = \frac{1}{V}\frac{\partial E}{\partial \gamma}, \tag{5}$$

as well as the normal stress, given by

$$\sigma_{zz} = \frac{1}{V}\frac{\partial E}{\partial \alpha}, \tag{6}$$

where V is the volume of the box, E is the network energy, and α is a superimposed, virtual uniaxial strain in the z direction—the direction perpendicular to the shear. In detail, each step consists of an affine displacement of all segments in the network to accommodate for the global shear, as well as evolution over the time increment Δt as specified in Eq. (3). Thus we simulate the network response under the assumption that in the limit of high frequencies the local shear deformation at any place in the network is equal to the global shear. In experiments, there might be shear banding or similar effects that lead to a nonuniform distribution of the bulk strain over the cross section of the sample—we do not capture such effects.

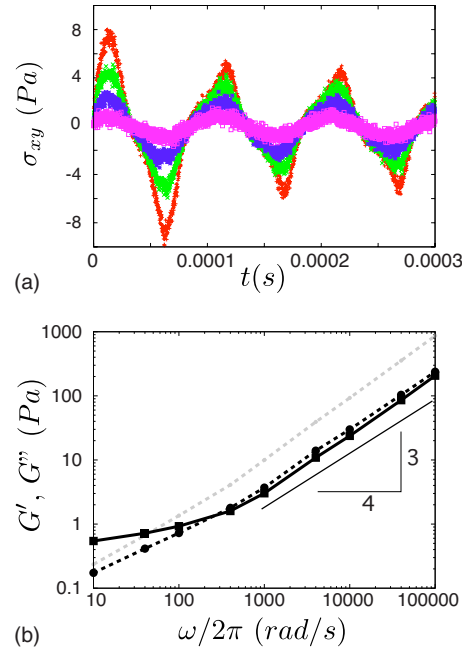

FIG. 2. (Color online) The dynamical network response. (a) The shear stress σ_{xy} during oscillatory network shear with frequency $\omega = 2\pi 10^4$ rad/s, for shear amplitudes of $\gamma_0 = 0.02$, 0.06, 0.10, and 0.14. (b) Elastic modulus (solid black curve) and viscous modulus (dotted black curve) as a function of frequency. The dotted gray curve indicates the viscous modulus when the dynamical viscosity of the liquid is included. Data shown are averages over four networks realizations. Black line depicts an exponent of 3/4.

V. MEASUREMENTS OF G' AND G''

Figure 2(a) presents some typical curves of the shear-stress response on shearing, for different values of the shear amplitude γ_0 and a fixed frequency. In each simulation, we evolve the network over three full oscillations. As shown in this figure, small shear amplitudes give rise to a sinusoidal stress response, while with increasing shear amplitude the stress response becomes increasingly nonlinear (but less noisy), confirming experimental observations [20]. We compute the network moduli at shear amplitudes ranging from 0.02 for high frequencies up to 0.2 at low frequencies, each time making sure that we are still in the linear regime.

We fit the time-dependent stress with $\sigma_{xy}(t) = \sigma_0 \sin(\omega t + \delta)$ and obtain the elastic and viscous moduli respectively from $G' = \sigma_0/\gamma_0 \cos(\delta)$ and $G'' = \sigma_0/\gamma_0 \sin(\delta)$. Figure 2(b) shows the network moduli as a function of frequency. We see that the elastic modulus plateaus at low frequencies, and steeply increases for high frequencies. This is similar to what was reported both for experiments and similar simulations [9,15]. For the higher frequencies investigated, we find $G' \sim \omega^\alpha$, where α is larger than 3/4 as expected for the high-frequency limit [7]. Our data are more consistent with α

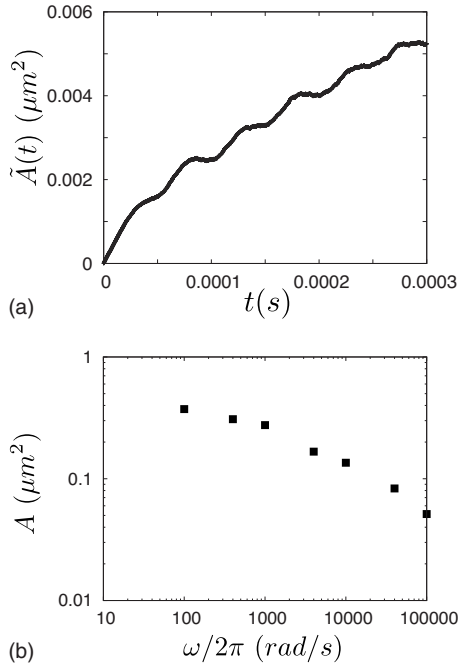

FIG. 3. The nonaffinity of the networks during oscillatory shear. (a) The nonaffine deformation $\tilde{A}(t)$, as defined in Eq. (7), for network oscillation with frequency $\omega=2\pi 10^4$ rad/s. (b) The shear nonaffinity A, as defined in the text, as a function of frequency. Data shown are averages over four networks realizations.

≈ 1. Even for the smallest strain amplitudes, which were used to calculate the network moduli, the stress response shows a slight decreasing trend with increasing number of oscillations; we verified, in longer simulations over nine oscillations for the higher frequencies, that this influences our measurements in Fig. 2(b) by at most 6%. Thus far, the shear viscosity due to the solvent is not included; it would simply contribute an extra stress term $\sigma_{xy}^{\eta}=\eta\dot{\gamma}$. This shear viscosity of the liquid affects only G'' and not G'. It does, however, trivially affect the crossover frequency where G'' and G' are equally large, as shown in Fig. 2(b). At high frequencies, as expected, the shear viscosity due to the solvent becomes the dominant contribution in G''.

VI. DYNAMICAL SUPPRESSION OF NONAFFINITY

Another aspect of the network response on oscillatory shear deformation is the nonaffine motion of components of the network. The nonaffinity is measured by

$$\tilde{A}(t)=\langle[x(t)-x(0)]^2\rangle, \tag{7}$$

evaluated at a given strain γ. This nonaffinity is plotted as a function of time in Fig. 3(a). We observe a global increase in the nonaffinity, accompanied by an oscillatory trend with a frequency directly related to the applied shear. We may in this case distinguish a thermal and a deformational component of the nonaffinity. Without shear, $\tilde{A}(t)$ simply measures the mean square displacement of a cross-linker, which at finite temperature will by itself produce a nonaffinity that increases with time. On top of that there is an oscillatory component tracking the externally imposed deformation. Thus far, the nonaffinity of a network has been tied uniquely to the bending dominated response of the filaments to a global shear deformation [12–14,18]. The figure, however, shows also a steadily increasing background nonaffinity on top of this contribution, caused by thermal fluctuations of the segments in the viscous medium. The contribution of these nonaffine motions can be large in comparison with the shear component of the nonaffinity. To the best of our knowledge, there is no general way to separate out the thermal component of the nonaffinity such that one measures only the nonaffinity due to shear; in simulations with thermal motion the filaments explore a large phase space, and the average position of the filaments depends largely on the time window of the simulations. It is important to realize that these thermal nonaffine fluctuations are not just an artifact of our method but a genuine phenomenon that will also be present in experiments. To characterize the frequency dependence of the shear component of the nonaffinity we calculate the average amplitude of the oscillations on top of the thermal nonaffinity, since these oscillations are a direct consequence of the oscillatory shear. To facilitate a comparison of the results for different frequencies, we divide this amplitude by the squared shear amplitude γ_0^2. This results in the shear nonaffinity measure A, similar to the one used in previous simulations and experiments [9,14,18]. A value of $A=1$ μm^2 means that the average nonaffine displacement at a shear of 1 equals 1 μm; note that this is not a special point. Figure 3(b) shows the shear nonaffinity as a function of frequency. As does the stress response, also the shear nonaffinity decreases slightly after the first couple of oscillations, by at most 25%. The data points at the lowest frequencies are omitted: for such low frequencies it becomes impossible to separate the oscillations from the thermal background nonaffinity.

Interestingly, we observe a decreasing shear nonaffinity with increasing frequency. Apparently, with increasing frequency the nonaffine relaxation of the network is increasingly prohibited. Prior simulations have revealed the relation between nonaffine reorientations and the network stiffness: nonaffine reorientations allow the networks to minimize their energy and, therefore, systems that can access all nonaffine modes are mechanically soft [18]. We conclude from Fig. 3(b) that with increasing frequencies the networks have less time to relax in this manner, which explains both the decreasing nonaffinity [Fig. 3(b)] and the increasing stiffness [Fig. 2(b)] with increasing frequency. In the following section we will put this relation between network stiffness and the nonaffinity in a broader perspective.

VII. CLASSIFICATION OF REGIMES

The current view presented in literature [7,9,21] is that there is a characteristic frequency ω_s, determined by the typical relaxation time of the single segments [see Eq. (4)]; above this frequency, the segments have no time to fully relax during the oscillatory shear, and the network is microscopically out of equilibrium. Assuming affine motion of the solvent, as is appropriate for small typical interplate distances, we assume that the network, too, will deform affinely

in this regime. The lack of single-segment relaxation results in a stiffening of the network modulus, which is both computed and measured to scale as $\omega^{3/4}$. Below this frequency, the single segments can relax, the network is assumed to deform affinely, and this yields a plateau in G'.

Our results show a richer picture, which also has some important differences. In agreement with the literature view, above ω_s the single segments are out of equilibrium and the network response is dominated by their behavior. We distinguish a second characteristic frequency $\omega_n < \omega_s$, set by the long wavelength modes of network deformation—those with the longest relaxation times. Between ω_n and ω_s, the single segments have time to relax, but the slowest network modes do not. Upon lowering the driving frequency, starting from ω_s, more and more network modes are able to relax during the oscillatory shear, and the elastic modulus G' will therefore slowly converge to its plateau value, but only reach this at ω_n when *all* modes are fully equilibrated. Because of the polydispersity of the segment lengths, there is no clean definition of ω_s; however, since the average segment length is 1 μm, typically the segments do no longer fully relax above $\omega_s \approx 50$ kHz (see also [7]). Similarly, because of the large distribution of the eigenfrequencies of the network [22], there is no clean definition of ω_n either. However, our guess for our networks would be around $\omega_n \approx 10$ Hz, since both G' in Fig. 2(b) and A in Fig. 3(b) start to saturate around this value. We find that for high frequencies $G \sim \omega^{\alpha}$ with $\alpha > 3/4$, whereas a response dominated by the single-segment relaxation would have $\alpha = 3/4$. Intuitively, it makes sense that with decreasing frequency the elastic modulus drops faster than expected purely on single-filament response: on top of the single-segment relaxation also the network relaxes more and more.

The nonaffinity follows an opposite trend. Starting from affine behavior at frequencies above ω_s, as more and more modes are able to relax from the affine deformation induced by the oscillatory shear, the nonaffinity will increase to its plateau value at slow shear. We know that the slow, low frequency modes are highly delocalized, while the fast, high-frequency modes are localized [22]. Therefore, both the amplitude and the spatial correlation of the nonaffine displacements will increase with decreasing frequency. Figure 4 illustrates this scenario of the three distinct regimes, by showing the nonaffine displacements during deformation of a two-dimensional network in each regime.

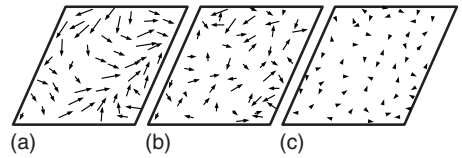

FIG. 4. An illustration of the network response in a (two-dimensional) network during shear. The arrows show the deviation from affine displacements of the cross-links. (a) At frequencies below ω_n, all network modes can fully relax. The deviation from affine displacement is large and spatially correlated. (b) At frequencies larger than ω_n the slowest (extended) network modes cannot relax but the localized (fast) network modes can, as well as the single-filament modes. The nonaffine displacements are smaller and no longer spatially correlated. (c) At frequencies above ω_s, both the localized network modes and the single-segment modes cannot relax and the network deforms more and more affinely.

VIII. LARGE SHEAR AMPLITUDES

So far, we studied the network response to oscillatory shear, in the regime of linear response. We now turn to a unidirectional constant shear rate up to a much larger shear amplitude of 0.5. We simulate the shear response for three different shear rates, namely $\dot{\gamma} = 10^2$ s^{-1}, 10^3 s^{-1}, and 10^4 s^{-1}, averaged over four different network realizations. In these calculations we leave out the dynamical viscosity of the liquid. Figure 5(a) shows the shear-stress response as a function of shear for these different shear rates. As can be seen, all networks show shear stiffening. With increasing shear rates the initial stiffness increases, as expected from the increasing elastic modulus with frequency in Fig. 2(b), and the onset of stiffening occurs at smaller strains γ. These results fit well to our picture for the small-strain regime. For low shear rates, the networks have a lot of time to accommodate the deformation, thus leading to a soft network response. Stretching of single segments can be postponed until large shears, which causes a late onset of stiffening. For large shear rates the times are too short to relax, leading to a stiff network response. The small strain at which the networks starts to stiffen indicates that the filaments get stretched already at small shears.

We also calculate the normal stress σ_{zz} during deformation as a function of shear. A negative normal stress is one of the hallmark features of nonlinear mechanical response in biopolymer networks [23]. We find that σ_{zz} is indeed negative and shows the same shear-rate dependence as the shear stress, see Fig. 5(b).

Because of symmetry, the shear stress and normal stress should be odd and even functions of the shear strain, respectively; Fig. 5(c) shows that this is the case in our simulations.

Our results may be relevant for the appropriate interpretation of nonlinear rheological data. Two methods have been developed to measure the differential stiffness at large strains and there has been some debate whether they will give the same results. One method measures the stiffness by superposing a small amplitude oscillatory shear $\partial\gamma$ for a constant applied shear γ [20]. This method allows for a relaxation of all network modes at the constant shear γ, after which the small amplitude oscillatory shear is applied. The alternative for measuring the large strain response is to apply a shear with constant shear rate [24]. Here, the shear rate determines whether the networks modes can or cannot relax. Although for slow deformation these two methods might give similar results, our results suggest that for fast deformation they will certainly not.

IX. RELATION TO PRIOR WORK

In the last decades, many simulational, modeling, and experimental efforts have focused on understanding the zero-frequency response of networks with fixed cross-links. These

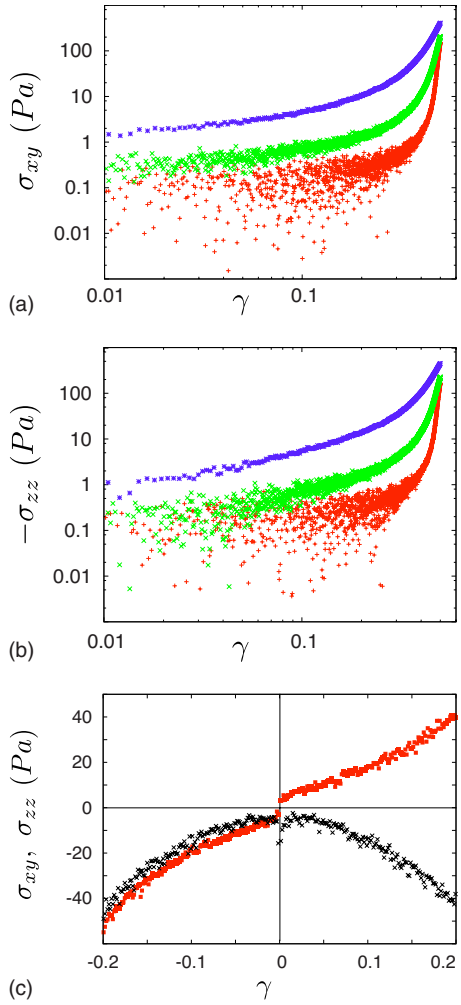

FIG. 5. (Color online) The network response for large shear. (a) The shear stress σ_{xy} as a function of shear, for three different (nonoscillatory) shear rates $\dot{\gamma}=10^2$ s^{-1} (lower), 10^3 s^{-1} (middle) and 10^4 s^{-1} (top curve). (b) The normal stress σ_{zz} as a function of shear, for the same three shear rates. (c) The shear stress (odd function of strain) and normal stress (even function of strain) for a network which is initially well relaxed at zero strain, and then subsequently sheared in the direction of positive as well as negative strain, at a shear rate of $\dot{\gamma}=10^4$ s^{-1}.

studies revealed that both the nonaffinity and the network stiffness depend strongly on the network geometry: increasing the number of cross-links per filament strongly decreases the floppiness of the structure and thus decreases the nonaffinity and increases the modulus. Another important parameter is the relative filament stiffness, captured well by the ratio between the persistence length and the segment length. Increasing this ratio increases the relative importance of the nonaffinity on the network response, and a low ratio implies floppy segments and thus a response that is dominated by an (affine) stretching of single segments [13,14,18,22,25,26]. Complementary to these dependencies on filament stiffness and network structure, in this work we presented the *frequency* dependence of the network modulus and the nonaffinity. This frequency dependence response related to the nonaffinity is mostly relevant for networks deforming highly nonaffinely in the zero-frequency limit. Clearly, networks deforming close to affinely in the zero-frequency limit will not show this characteristic nonaffine to affine transition for increasing frequencies. Note that the theory of the frequency dependent deformation by MacKintosh *et al.* [7] assumes affine behavior in the zero frequency limit, and thus does not apply to materials in which the zero-frequency behavior is nonaffine.

On the other side of the frequency spectrum, our current work is bounded from below by the work of Lieleg *et al.* [8], who consider the dynamical response of a network with cross-linkers that may bind and unbind. We do not consider this effect, as the time scale for such processes (typically $\omega < 1$ Hz) is generally larger than the characteristic time scales of the nonaffine reorientations.

A similar simulation method has recently been proposed and implemented by Kim and co-workers [15] to study the viscoelastic response of actin networks. Our work differs from theirs in several important respects: we distinguish different components of the drag coefficient, take into account the full force extension curve of individual segments and measure the dynamic nonaffinity. Interestingly, they observe a similar increase in the network modulus with increasing frequency in networks with zero prestrain. In the highly prestrained networks they proceed to consider, the frequency dependence of the elastic modulus vanishes. This is exactly the behavior we expect for a network that loses the configurational freedom to relax by nonaffine reorientations due to the high prestresses in the filaments.

X. SUMMARY AND CONCLUSIONS

In summary, we have developed a simulation approach to study the response of cross-linked networks of biopolymers to dynamical shear. Our main finding is that at low frequencies, all network modes and single-filament modes are free to relax and consequently the network will deform nonaffinely such that the networks are soft. With increasing frequencies the externally imposed strain outruns the internal relaxation modes, the nonaffinity decreases and consequently the network stiffens. At even higher frequencies, beyond those studied here, even the single-segments modes can no longer relax fully, and the network response is dominated by the single-segment relaxation. While the transition itself is generic, its exact location in frequency space is not—we find that this is highly sensitive to filament and network parameters such as the persistence length, the density and average length of filaments, and the viscosity of the medium.

[1] B. Alberts, A. Johnson, J. Lewis, M. Raff, K. Roberts, and P. Walter, *Molecular Biology of the Cell*, 5th ed. (Garland Science, New York, NY, 2008).
[2] H. Lodish, A. Berk, S. L. Zipursky, P. Matsudaire, D. Baltimore, and J. Darnell, *Molecular cell biology*, 4th ed. (W.H. Freeman and Company, New York, 2000).
[3] P. A. Janmey, S. Hvidt, J. Lamb, and T. P. Stossel, Nature (London) **345**, 89 (1990).
[4] L. Deng, X. Trepat, J. P. Butler, E. Millet, K. G. Morgan, D. A. Weitz, and J. F. Fredberg, Nature Mater. **5**, 636 (2006).
[5] S. Yamada, D. Wirtz, and S. C. Kuo, Biophys. J. **78**, 1736 (2000).
[6] K. E. Kasza, A. C. Rowat, J. Liu, T. E. Angelini, C. P. Brangwynne, G. H. Koenderink, and D. W. Weitz, Curr. Opin. Cell Biol. **19**, 101 (2007).
[7] F. Gittes and F. C. MacKintosh, Phys. Rev. E **58**, R1241 (1998).
[8] O. Lieleg, M. M. A. E. Claessens, Y. Luan, and A. R. Bausch, Phys. Rev. Lett. **101**, 108101 (2008).
[9] G. H. Koenderink, M. Atakhorrami, F. C. MacKintosh, and C. F. Schmidt, Phys. Rev. Lett. **96**, 138307 (2006).
[10] F. Gittes, B. Schnurr, P. D. Olmsted, F. C. MacKintosh, and C. F. Schmidt, Phys. Rev. Lett. **79**, 3286 (1997).
[11] F. Amblard, A. C. Maggs, B. Yurke, A. N. Pargellis, and S. Leibler, Phys. Rev. Lett. **77**, 4470 (1996).
[12] J. Wilhelm and E. Frey, Phys. Rev. Lett. **91**, 108103 (2003).
[13] D. A. Head, A. J. Levine, and F. C. MacKintosh, Phys. Rev. E **68**, 061907 (2003).
[14] E. M. Huisman, T. van Dillen, P. R. Onck, and E. Van der Giessen, Phys. Rev. Lett. **99**, 208103 (2007).
[15] T. Kim, W. Hwang, H. Lee, and R. D. Kamm, PLOS Comput. Biol. **5**, e1000439 (2009).
[16] C. Storm, J. J. Pastore, F. C. MacKintosh, T. C. Lubensky, and P. A. Janmey, Nature (London) **435**, 191 (2005).
[17] J. Wilhelm and E. Frey, Phys. Rev. Lett. **77**, 2581 (1996).
[18] E. M. Huisman, C. Storm, and G. T. Barkema, Phys. Rev. E **78**, 051801 (2008).
[19] M. Doi and S. F. Edwards, *The Theory of Polymer Dynamics* (Oxford University Press, Oxford, 1986).
[20] M. L. Gardel, J. H. Shin, F. C. MacKintosh, L. Mahadevan, P. Matsudaira, and D. A. Weitz, Science **304**, 1301 (2004).
[21] D. C. Morse, Phys. Rev. E **58**, R1237 (1998).
[22] E. M. Huisman and T. C. Lubensky (unpublished).
[23] P. A. Janmey, M. E. McCormick, S. Rammensee, J. L. Leight, P. C. Georges, and F. C. MacKintosh, Nature Mater. **6**, 48 (2007).
[24] R. Tharmann, M. M. A. E. Claessens, and A. R. Bausch, Phys. Rev. Lett. **98**, 088103 (2007).
[25] J. Liu, G. H. Koenderink, K. E. Kasza, F. C. MacKintosh, and D. A. Weitz, Phys. Rev. Lett. **98**, 198304 (2007).
[26] C. Heussinger and E. Frey, Phys. Rev. E **75**, 011917 (2007).